Computational study of stratified charge compression ignition engines with late injection under low-load conditions

H. Zhang [a,*], E. R. Hawkes [a,b], S. Kook [b], W. Hwang [c]
[a] School of Photovoltaic and Renewable Energy Engineering,
The University of New South Wales, Australia
[b] School of Mechanical and Manufacturing Engineering,
The University of New South Wales, Australia
[c] GE Global Research, U.S.A
haoyang.zhang@unsw.edu.au, evatt.hawkes@unsw.edu.au,
s.kook@unsw.edu.au and hwang@ge.com

Abstract

The fuel stratification introduced by direct injection (DI) of iso-octane in an optically accessible homogeneous charge compression ignition (HCCI) engine is numerically investigated by using a multi-dimensional model. The primary purpose of this study is to provide an understanding of the effects of late DI on the in-cylinder fuel-air mixture distribution under low-load conditions. It is well known that combustion efficiency is rather low and the associated carbon monoxide (CO) and unburned hydrocarbons (uHC) emissions are quite high for HCCI engines operated at low-load. DI has the potential to improve the combustion efficiency and reduce emissions by introducing charge stratification to increase local combustion temperatures. To understand and optimize performance, detailed transient information about in-cylinder flow motions, fuel-air mixing, and mixture distributions is required. In this study, the model is validated by comparing the fuel distributions between calculations and measurements made using planar laser induced fluorescence at three different injection timings. Then, it is used to investigate the effects of swirl ratio, injection pressure and included angle of the spray on the fuel distributions after the compression stroke. It is found that the predicted fuel distributions are in a good agreement of with measurements, and that the model is able to reproduce the phenomena observed in the experiments.

Introduction

Homogeneous charge compression ignition (HCCI) engines have the potential to improve fuel-consumption economy relative to spark-ignition engines, to reduce particulate emissions relative to diesel engines and to reduce nitrogen oxides (NO_x) relative to both spark-ignition and diesel engines [1]. However, low combustion efficiency at low loads and associated high levels of carbon monoxide (CO) and unburned hydrocarbons (uHC) emissions pose serious challenges for practical applications [2-6]. Dec and Sjöberg [3] have demonstrated experimentally that the high CO and uHC emissions were caused by incomplete bulk-gas reactions at low-load (equivalence ratio, Φ, below 0.2) operations, and charge stratification by late direct injection (DI) was found to be beneficial for improving combustion efficiency at those loads by concentrating the fuel in the central regions of the combustion chamber, leading to a locally less dilute mixture. Hwang *et al.* [6] investigated the influence of the type of fuel injector, injection pressure, and in-cylinder swirl on charge stratification. Images of the local equivalence ratio were produced using planar laser induced fluorescence (PLIF) to better understand the differences in mixture formation under various injection parameters and operating conditions. However, those measurements were taken on two-dimensional planes so that instantaneous information about in-cylinder flow motions, fuel-air mixing, and mixture distributions cannot be provided. Based on those experiments, Abraham [7] numerically investigated the effect of injector hole-size, number of holes, injection parameters, and in-cylinder swirl on fuel stratification. However, only qualitative results were supported, without direct comparison with experimental measurements. Hence, it would be useful to provide such more detailed in-cylinder information with quantitative accuracy. Few prior researches (to authors' best knowledge) attempt to quantitatively compare in-cylinder fuel distributions obtained from models and experiments in a HCCI engine, so this is the aim of this study.

In the present study, numerical experiments were conducted by using a multi-dimensional model to reproduce the PLIF measurements of fuel distributions by Hwang *et al.* in ref. [6]. The paper firstly describes the modelling configurations used. Then, comparisons between calculations and experiments under different injection timings and various injection parameters are presented.

* Corresponding author: haoyang.zhang@unsw.edu.au; jerry.haoyang.zhang@gmail.com

Numerical Methods

The commercial computational fluid dynamics (CFD) package ANSYS-CFX v13.0 was employed. This package applies the finite volume method to solve the conservation equations. A transient Reynolds-Average Navier-Stokes (RANS)-based model was employed to conduct the numerical experiments. A second order scheme was used for all equations including the turbulence and species transport equations.

Detailed descriptions of the engine geometry are available in ref. [3, 6], and simplified specifications were summarized in Table 1. Note that in order to match the top dead center (TDC) pressure of the optical engine experiment under the boosted intake pressure and temperature, the compression ratio (CR) used in the CFD model was reduced to 12.8 (from 14.0). This change was necessary because the model does not include some loss mechanisms, notably blow-by. Simulations started from the time of intake valve closure (205^o crank angle) and were advanced up to 5^o crank angle (CA) after TDC, *i.e.* 365^o CA. The detailed flow in the intake and exhaust ports and valves was not modelled, in part due to some geometrical information being unavailable. Effects of the intake flow were only included by a specified swirl number of the in-cylinder flow. Therefore, the geometry considered was simple cylinder with a flat piston and roof, and a small crevice volume. Furthermore, computations were carried out in a 45^o sector since the 8-hole injector used in the experiments was considered as having a sector-to-sector symmetry in the modelling, *i.e.* the spray from each hole was assumed to be identical. Figure 1 (a) shows the initial 3-dimensional grid that was built with ANSYS ICEM-CFD. The grid (baseline mesh) contained 102,600 elements, and consisted of the central zone meshed with 1,800 wedges (only the first grid on the centreline) and other parts meshed with 100,800 hexahedra. All surfaces were set as the boundary condition of wall, except two side surfaces being symmetric.

Table 1 Optical HCCI engine specifications

Displacement (single-cylinder)	0.981 litre	Intake Valve Close (IVC)	205^o CA**
Bore	102 mm	Swirl Ratio	1.3
Stroke	120 mm	Engine Speed	1200 rpm
Connecting Rod Length	192 mm	Intake Pressure	135 kPa
Geometric Compression Ratio	14:1*	Coolant Temperature	100^o C
Clearance Volume Height	8.05 mm		

* It was adjusted to 12.8:1 in the CFD model.

** 360^o CA is TDC of compression.

A grid independence study was carried out. Detailed comparisons will be discussed in next section. The effects of time-step and number of particles (parcels) were also studied. A time-step of 0.1 CA was selected and a time-step of 0.01 CA was used during injection and evaporation processes. The number of approximately 30,000 parcels was found to be sufficient to represent the spray.

A specified in-cylinder flow velocity profile was employed to assign an initial swirl flow with the same swirl ratio (SR) as that used in experiment (*i.e.* SR=1.3). The swirl ratio was determined by using the paddle wheel model [8], *i.e.* defined by the ratio of the angular velocity of the fluid in the cylinder to the crank shaft angular rotational speed (1200 rpm in this study).

Turbulence was modelled using a Re-Normalized Group (RNG) k-ε model. The default model constants provided by CFX were used [9] and a scalable wall-function was adopted [10]. The fractional turbulence intensity was initialized as 0.1 and the eddy length scale was set initially to be 10% of the engine bore. A constant wall temperature of 373.15 K was used. Although the constant wall temperature is less justifiable even for non-reacting simulations, cases with non-constant wall temperatures at cylinder head, liner and piston whose values were estimated from the measured firedeck temperature from the experiments [16] were also examined. It was found that the heat transfer between walls and bulk-gas barely affected fuel evaporation and mixture distribution. Hence, the constant wall temperature was maintained. The initial temperature of the bulk-gas was set to match the intake temperature used in the experiments.

Iso-octane was used as the fuel, and the fuel temperature before injection was set equal to the coolant temperature (373.15 K). Fuel properties, such as surface tension and liquid density, were adjusted corresponding to liquid fuel temperature. Three injection timings were selected to establish baseline cases compared to the experiments, namely, with a start of injection (SOI) of 290^o CA, 315^o CA, and 330^o CA, respectively. The fuel injection was modelled by using the blob injection method [10], in which the initial spherical droplets with uniform size of the nozzle size (*i.e.* 0.125 mm in this study) are injected that are subject to aerodynamic induced secondary breakup. The Reitz and Diwakar breakup model [10-11] was used for the secondary breakup model. This model distinguishes between two breakup regimes: bag breakup and stripping breakup. Breakup takes place if a critical particles Weber number has been exceeded. Independent of the breakup regime, the reduction of the particle radius during breakup is described as

$$\frac{dr_P}{dt} = \frac{-\left(r_P - r_{stable}\right)}{t_{br}}, \tag{1}$$

where r_P is the droplet radius prior to breakup, r_{stable} is the new radius for the stable droplet and t_{br} is the characteristic breakup time. Values for r_{stable} and t_{br} are computed from the equations given in the following:

For bag breakup, $\left(We > We_{crit}\right)$

$$t_{br} = C_1\sqrt{\frac{\rho_P r_P^3}{2\sigma}} \quad \text{and} \quad r_{stable} = \frac{6\sigma}{\rho_F V_{slip}^2}, \tag{2}$$

For stripping breakup, $\left(We/\sqrt{\mathrm{Re}} > C_{s1}\right)$

$$t_{br} = C_2\frac{r_P}{V_{slip}}\sqrt{\frac{\rho_P}{\rho_F}} \quad \text{and} \quad r_{stable} = \frac{\sigma^2}{2\rho_F^2 V_{slip}^3 \nu}, \tag{3}$$

where ρ_P is the density of the particle, ρ_F is the density of the surrounding fluid, σ is the surface tension, ν is the kinematic viscosity of the surrounding fluid and V_{slip} is the relative velocity between the particle and the surrounding fluid. The Weber number $We = \rho_F V_{slip}^2 r_P/\sigma$ and the Reynolds number $\mathrm{Re} = 2V_{slip}r_P/\nu$. The model constants $C_1 = \pi$, $C_2 = 8$, $We_{crit} = 6.0$ and $C_{s1} = 0.5$ were used in this study.

The effect of cavitation on atomization was not considered. The Ranz-Marshall model [9] and Schiller-Naumann model [9] were used to account for particle heat transfer and momentum transfer, respectively. A liquid evaporation model [9] and the Sommerfeld particle collision model [9] were applied. Non-drag forces, including the virtual mass force, turbulent dispersion force, and pressure gradient force were considered.

The amount of injected fuel corresponded to a global Φ equal to 0.12, and an injection pressure of 120 bar was employed. The mass flow rate of fuelling was calculated as [12-13]:

$$\dot{m}_f = C_a \cdot A_f \cdot \rho_f \cdot C_v \cdot U_b \quad \text{and} \quad C_d = C_a \cdot C_v, \tag{4}$$

where the velocity U_b is the maximum potential fluid velocity, given by Bernoulli's equation:

$$U_b = \sqrt{2\cdot(P_f - P_a)/\rho_f}\,. \tag{5}$$

Here, the term A_f is the orifice exit area, ρ_f is the fuel density, and P_f and P_a are the fuel and ambient gas pressures, respectively. The velocity coefficient is denoted as C_v and the product $C_v \cdot U_b$ (the average velocity) was used as the injection velocity. The orifice area-contraction coefficients is denoted as C_a, and $C_a = 1.0$ was used in this study. It should be noted that $C_a = 1.0$ was reasonable to use in the numerical study since the blob method was applied and no cavitation was considered. The discharge coefficient $C_d = 0.8$ was applied, implying $C_v = 0.8$.

Results and Discussion

Figure 2 shows a comparison between calculations and experiments of the fuel-air mixture distribution at 365° CA (at the end of simulation) at different injection timings on the plane 4 mm below the cylinder head as shown in Fig 1 (b). For the simulations, mass-weighted histograms were obtained based on the density-weighted equivalence ratios on the same plane as the experiments. It can be seen in Fig. 2 that although there are some discrepancies, CFD calculations show an overall good agreement with the experiments for the fuel distributions at three different injection timings. In the experiments, at early injection (SOI=290° CA) DI created large regions with local Φ>0.14 which would result, if homogeneous, a combustion efficiency of about 70% [6], compared to premix charge in conventional HCCI. That led to a significant increase of local combustion temperature and overall combustion efficiency. As injection was further delayed (SOI=315° and 330° CA), the experiments showed that more regions with Φ>0.2, which was required for complete combustion [6], were created in the central area of the cylinder, resulting in significant reduction of CO and uHC emissions. In the modelling, the calculations demonstrate a good agreement with the observations in the experiments, *c.f.* Fig. 2.

At SOI=290° CA in Fig. 2, despite the fact that the model slightly over-predicted the extent of relatively leaner regions and under-estimated the extent of the richer regions, the model performed well over a good range of equivalence ratios. The disparities could be caused by approximations made to set the initial flow conditions since for this early injection timing, there was significant time for the fuel spray to interact with the bulk-gas flow and turbulence. Moreover, the intensity of turbulence was set empirically. The same reason might have also contributed to the over-prediction of the relatively leaner regions at SOI=315° CA in Fig. 2 as well.

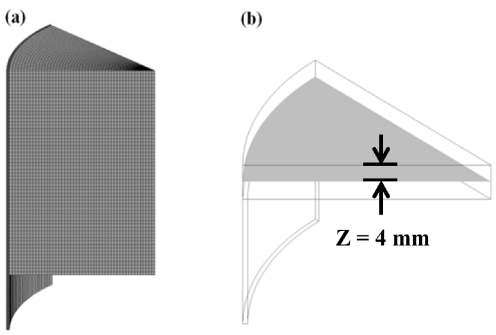

Figure 1 (a) 3-Dimensional grid layout at the start of simulation; (b) the plane used to obtain the fuel distribution at the end of simulation.

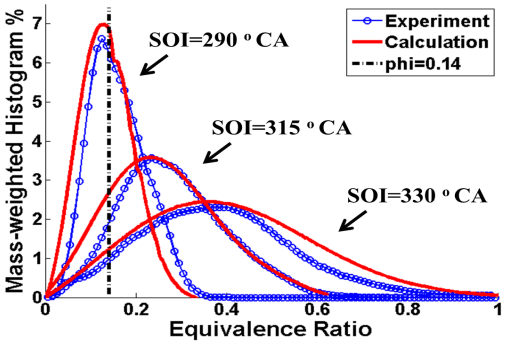

Figure 2 Mass-weighted histogram of fuel-air mixture on the plane 4 mm below the cylinder head as a function of equivalence ratio.

Vertical stratification of the fuel distribution at SOI=315° CA was investigated by comparing the Φ-map at a lower elevation, *i.e.* at a plane 6 mm below the cylinder head. Compared to the Φ-map on the 4 mm mid-plane in Fig. 3 (a), the overall fuel distribution at 6 mm plane in Fig. 3 (b) is similar, while the lower elevation exhibits a slighter higher fuel concentration, as shown in Fig. 4. Figure 4 shows the comparison of fuel distributions between calculations and experiments at both planes. It can be seen in Fig. 4 that the model shows a good agreement with experimental data at both planes and gives a better lower elevation. Therefore, it confirms the existence of the fuel stratification on the vertical direction as shown in the experiments [6]. The existence of higher concentrations near the piston indicates that more NO_x could be generated in these regions, since NO_x emission could become significant when the local Φ>0.6 according to ref. [6].

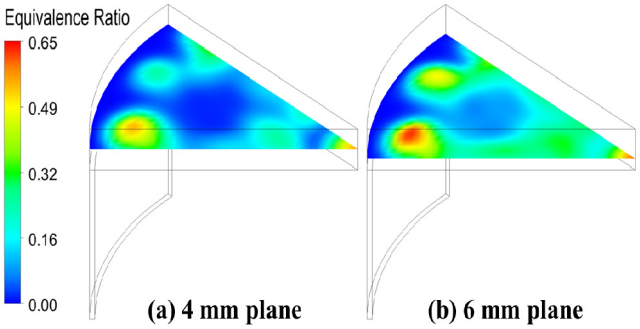

Figure 3 (a) Fuel distribution on the plane 4 mm below the cylinder head (mid-plane at TDC); (b) Fuel distribution on the plane 6 mm below the cylinder head.

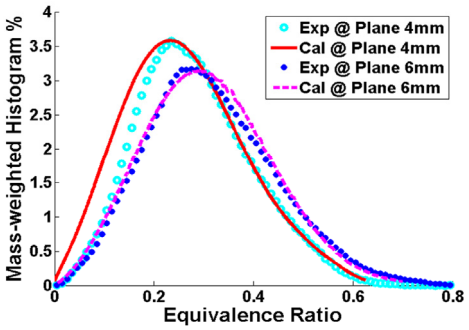

Figure 4 Comparison of fuel distributions at SOI=315°CA at the plane 4mm and 6 mm below the cylinder head.

At the later injection of SOI=330° CA in Fig. 2, the model over-estimated the fuel-rich regions somewhat. This might be due to limitations of the wall-particle impingement model used. Figure 5 shows spray structure at the end of injection at different injection timings. It can be clearly seen that particles hit the piston for the case with SOI=330° CA in Fig. 5 (b) but not for the other injection timing, *i.e.* SOI=290° CA in Fig. 5 (a). In the experiments, a wall-film might be formed at SOI=330° CA. In the modelling, the particle-wall interaction was modeled by assuming that the momentum change across the collision was elastic. A so-called quasi static wall film model was used [9] which neglects the wall film movement due to external forces. Wall particles interact only with their surroundings via mass transfer (evaporation) or heat transfer (wall conduction, convection). When the particles contacted with the piston wall in the modelling, they bounced after hitting the wall [9] and only small portion formed the wall film, since their temperatures were about 80 K hotter than the piston wall due to heat-up by surrounding hot air and the diameters of those particles near the piston were quite small due to break-up and evaporation. The bounced droplets increased upward fuel vapor penetration, leading to a dense region away from the piston. As a result, the calculation predicted high probabilities on the fuel-rich side, but overall the range of equivalence ratio of mixture matched quite well.

The effect of refinement of grid size was investigated. Figure 6 shows the comparison of the fuel distributions among the baseline mesh, fine mesh and experiments on the mid-plane. The fine mesh was refined by doubling the number of elements used in the computations. It can be seen in Fig. 6 that good grid independence is achieved. At SOI=290° CA in Fig. 6, the modelled fuel distribution was closer to the experimental data since the

Eulerian phase was better resolved. For SOI=315° and 330° CA in Fig. 6, the results were comparable between the two grids, but the probability of fuel-rich regions was over-estimated slightly more in the fine grid compared with the baseline grid. It was found that the refined grids near the injector (the location was shown in Fig. 5) interfered with the implicit assumption for the Lagrangian discrete phase that the volume fraction within a computational grid should be less than 0.1 [14-15]. It also should be mentioned that moving mesh configuration in ANSYS-CFX, particularly compression in this study, is based on the mesh deformation by specifying the displacements relative to the initial mesh. Consequently, the grid size on the vertical direction becomes smaller as the piston boundary moves up. On one hand, it may be beneficial for resolving the breakup and evaporation of the spray. On the other hand, it causes further decrease of grid size, raising the potential conflict with the Lagrangian assumption. Moreover, the computational cost for the fine mesh was almost tripled compared with that for the baseline mesh. Hence, the baseline mesh was used for all numerical experiments in this study.

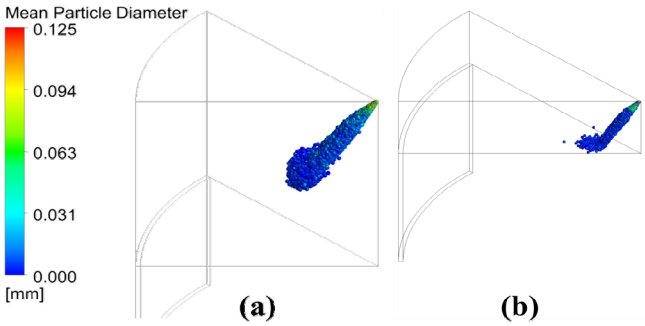

Figure 5 Spray structure at the end of injection at (a). SOI=290° CA and (b). 330° CA.

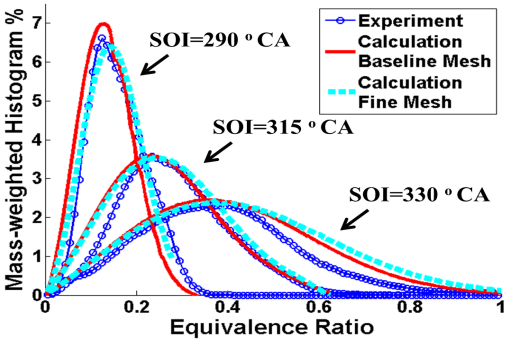

Figure 6 Comparison of fuel distributions between baseline mesh and fine mesh.

The experimental results were limited to a 2-D plane and the field of visible view. Based on the above validations of the model, it was reasonable to employ the model to further investigate the fuel distribution in the entire domain. Volume rendering of fuel distributions at 365° CA at three different SOI (baseline conditions) are shown in Fig. 7 (a-c). It can be seen that as the injection is retarded, *i.e.* from Fig. 7 (a) to (c), the fuel vapor becomes more concentrated in the central regions. Also, it may be observed that at SOI=290° CA in Fig. 7 (a), the mixture was relatively well mixed. However, the richest mixture was located in the crevice, where the temperature was much lower than the central regions. It can be speculated that if fired, this fuel would likely lead to deteriorated combustion efficiency and increased the emissions of CO and uHC. As the injection timing was retarded to 315° CA or later, there basically was no fuel located in the crevice, leading to potential reduction of CO and uHC emissions.

Furthermore, the main charge (the domain excluding the crevice volume) became denser as the injection was retarded. As mentioned before, Φ>0.2 was required for complete combustion and more regions with Φ>0.14 were expected for high combustion efficiency as shown in the experiments [6]. At SOI=290° CA in the modelling, *c.f.* Fig. 7 (a), large proportion of fuel distributed in the crevice volume, resulting in the main charge being too lean to complete the combustion. Hence, the proportion of the local mixture with Φ<0.2 (*i.e.* the regions could lead to incomplete combustion) was calculated for the modelling results based on the mass-weighted histogram of fuel-air mixture in the main charge at different SOI. The integrated area under the histogram curve (for the main charge part only) from Φ=0 to Φ=0.2 was compared with the total area under the curve. It was found that there was 80.1% mixture in the main charge with Φ<0.2 at SOI=290° CA in Fig. 7 (a). That proportion was significantly reduced to 26% and 11.2% when the injection was delayed to SOI=315° CA and SOI=330° CA, *c.f.* Fig. 7 (b) and (c), respectively. Therefore, those explain how CO and uHC emissions could be reduced to a much lower level compared with the earlier injection case, and the combustion efficiency could be significantly improved as the injection was retarded.

On the other hand, NO_x emission could become rather high for the later injection timings if fired, since the maximum equivalence ratio (Φ_{max}) predicted was 0.71 at SOI=315° CA in Fig. 7 (b). According to ref. [6], it was found in the experiments that NO_x emissions were increased considerably after SOI=315° CA. In the modeling, although some regions with Φ>0.6 were observed at SOI=315° CA in Fig. 7 (b), those regions were mainly located close to the piston, so that the local combustion process would be strongly affected by the wall quenching and cooling, probably leading to less NO_x production if fired. Hence, NO_x emissions at SOI=315° CA can still remain acceptable. As the injection was, however, further delayed, *i.e.* SOI=330° CA in Fig. 7 (c), the mixture became too richer at the central regions, potentially resulting in more NO_x emissions when combustion is involved. Hence, the modelling results confirmed that there was a tradeoff between combustion efficiency and NO_x, which was found in the experiments [6].

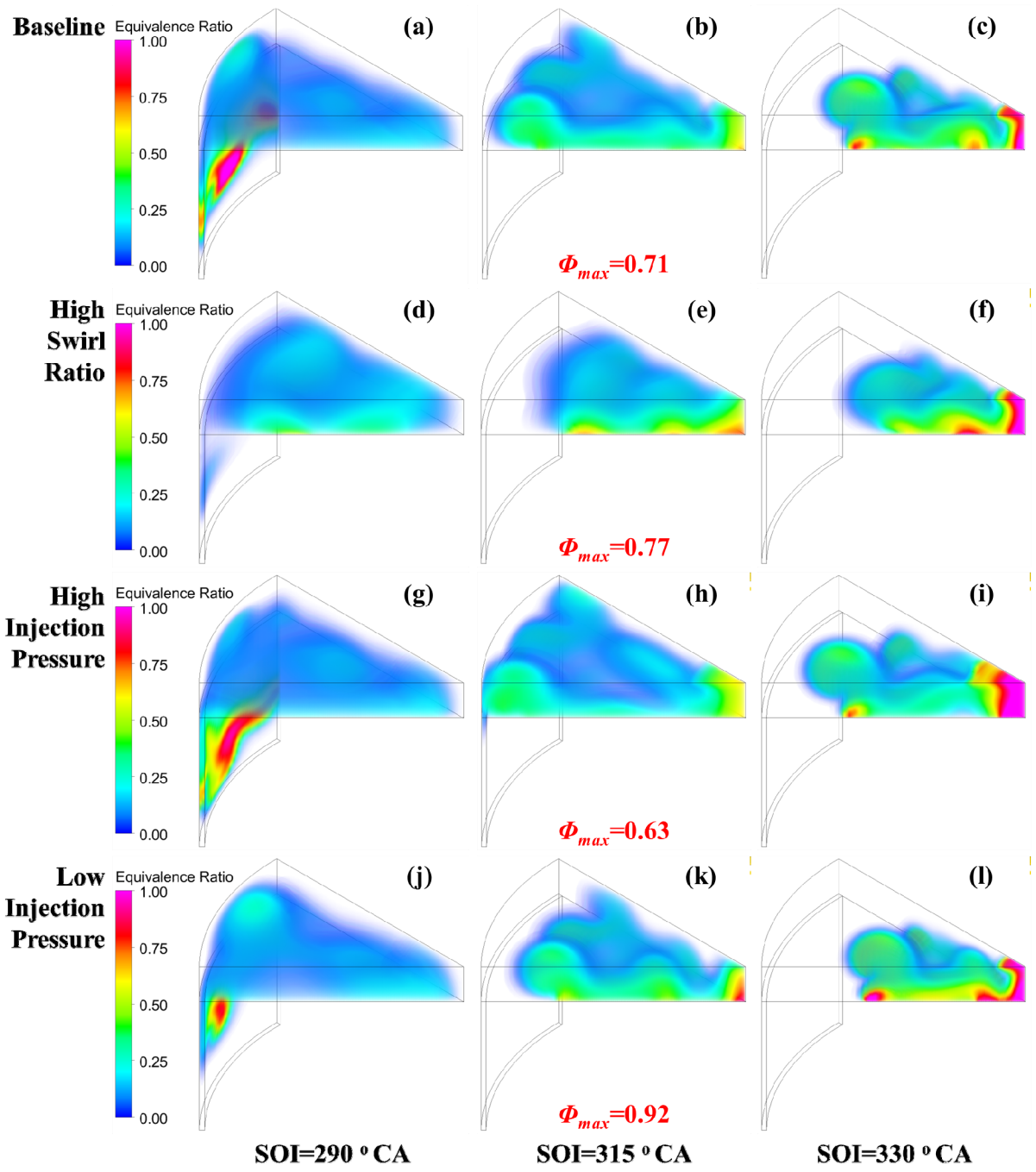

Figure 7 Volume rendering of fuel distributions under different injection parameters: 1st row: Baseline (P_{inj}=120 bar & SR=1.3); 2nd row: High swirl ratio (P_{inj}=120 bar & SR=3.6); 3rd row: High injection pressure (P_{inj}=170 bar & SR=1.3); 4th row: Low injection pressure (P_{inj}=70 bar & SR=1.3) at SOI=290° CA (1st column), SOI=315° CA (2nd column) and SOI=330° CA (3rd column).

Then, the model was used to investigate the effect of injection parameters on the improvement of combustion-efficiency/NO_x tradeoff. In the experiments, it was found that the combustion-efficiency/NO_x tradeoff generally improved when fuel can be injected as late as possible with acceptable levels of NO_x [6]. Therefore, techniques that can provide even faster mixing have the potential for further improvements. In the modelling, since no combustion was modelled in this study, direct comparison between combustion efficiency and NO_x emissions was unfeasible. In addition, it was found in the experiments that the possibly latest injection timing with acceptable NO_x emissions under baseline conditions was at SOI=315° CA [6]. Hence, the criterion of determining whether the tradeoff can be improved or not for the modelling results was to compare the predicted Φ_{max} in the domain at SOI=315° CA under the studied conditions with that of the modelled baseline conditions at SOI=315° CA, which was 0.71 as shown in Fig. 7 (b). It can be expected that if the predicted Φ_{max} under the studied condi-

tion was less than the criterion (Φ_{max}=0.71), the injection can be further retarded, *i.e.* later than 315° CA (to further increase the combustion efficiency) and NO_x emissions could still remain acceptable, leading to improvement of combustion-efficiency/NO_x tradeoff; while, if the predicted Φ_{max} was greater than the criterion, meaning that the injection timing had to be advanced so as to maintain NO_x emission being acceptable, resulting in detrimental to the tradeoff.

The fuel distributions under high swirl ratio (SR=3.6), high injection pressure (P_{inj}=170 bar), low injection pressure (P_{inj}=70 bar) and different included angles of the spray (θ) have been studied. In the experiments for 8-hole GDI injector, it was found that using high injection pressure improved the combustion-efficiency/NO_x tradeoff, while increased swirl was slightly detrimental to that tradeoff, and a low injection pressure showed a worse negative effect [6]. The model captured those observations accurately.

Figure 7 (d-f) show the volume rendering of fuel distributions under high swirl ratio condition. It can be seen that the local mixing at early injection, *i.e.* SOI=290° CA in Fig. 7 (d), was enhanced and less fuel located in the crevice due to increased swirl, compared to those in Fig. 7 (a). However, the global mixing rate at later injection timing, *c.f.* Fig. 7 (e-f), was lowered, compared to Fig. 7 (b-c), perhaps contrary to expectations. The fuel vapor penetration in Fig. 7 (e) was decreased compared to that in Fig. 7 (b), and the mixture appeared trapped by intensified swirl. Consequently, regions with Φ>0.6 were slightly more prevalent than in the low swirl ratio case (baseline condition), leading to Φ_{max}=0.77 at SOI=315° CA *c.f.* Fig. 7 (e). Hence, it can be speculated based on the predicted Φ_{max} that a high swirl ratio (SR=3.6) can be slightly detrimental to the combustion-efficiency/NO_x tradeoff, since NO_x emissions at SOI=315° CA under this condition *c.f.* Fig. 7 (e) could be excessive, so that the latest injection timing would be advanced to reduce NO_x emissions, causing a potential decrease of combustion efficiency.

Figure 7 (g-i) show the cases at different SOI under high injection pressure. Compared to Fig. 7 (a-c), the vapor penetration in Fig. 7 (g-i) was slightly enhanced at respective SOI due to higher injected momentum. While, the mixing rate at SOI=315° CA in Fig. 7 (h) was much improved, compared to Fig. 7 (b), leading to Φ_{max}=0.63. That could reduce NO_x emissions compared to that in Fig. 7 (b), so that the injection could be further retarded to achieve higher combustion efficiency.

Figure 7 (j-l) show the cases with a low injection pressure. Compared to Fig. 7 (b), it can be seen in Fig. 7 (k) that mixing became considerably worse and fuel-rich regions were much more prevalent at SOI=315° CA, leading to Φ_{max}=0.92. That could increase NO_x emissions significantly, so that much earlier injection timing would be required. Therefore, it can be speculated based on the modelled Φ_{max} that the combustion-efficiency/NO_x tradeoff could be improved by using a high injection pressure (P_{inj}=170 bar), while it could be deteriorated by a low injection pressure (P_{inj}=70 bar), compared to the baseline case with P_{inj}=120 bar.

The model was also used to investigate the effect of included angle of the spray (θ). According to ref. [6], the 8-hold injector used in the experiments had a θ=70° included angle. Figure 8 shows the spray structures at the end of the injection at SOI=290° CA under different included angles of the spray, *i.e.* θ=100° and θ=40°. It can be seen that a high included angle of the spray, *c.f.* Fig. 8 (a), prolonged the particle travel distance (closer to the cylinder wall), so that the possibility of that more fuel entering the crevice volume was increased. With a low included angle *c.f.* Fig. 8 (b), the spray showed the stronger influences of the bulk-gas motion (swirl) and the piston movement (squish flow). More fuel was likely to be re-bouncing back to near the centre-line after hitting the piston.

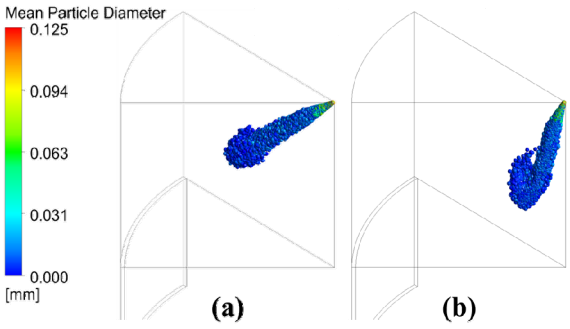

Figure 8 Spray structure at the end of injection at SOI=290° CA under (a) High included angle (θ=100°); (b). Low included angle (θ=40°).

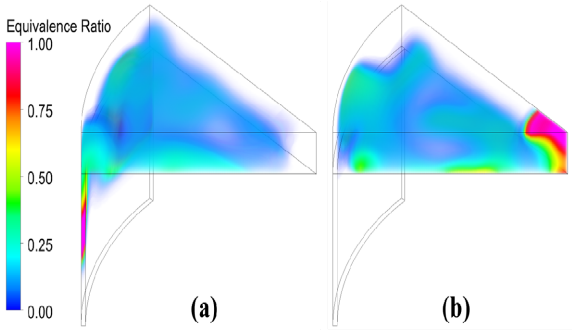

Figure 9 Fuel distribution at SOI=315° CA under (a) High included angle (θ=100°); (b). Low included angle (θ=40°).

Figure 9 shows the fuel distributions at SOI=315° CA under both included angles of the spray. It can be seen in Fig. 9 (a) that there was a large proportion of the fuel locating in the crevice even at SOI=315° CA under a high included angle of the spray, resulting in the main charge being rather lean. It was found that the proportion of the mixture with Φ<0.2 in the main charge in Fig. 9 (a) was 61.2%. Compared with that in Fig. 7 (b) which

was 26%, the combustion efficiency under a high included angle could be significantly reduced. Although the combustion efficiency could be potentially improved by further delaying the injection under high included angle condition, by examining the mixture with Φ<0.2 in the main charge at SOI=330^o CA under high included angle condition (not shown in here), it was found that there still was 29.5% mixture being too lean to complete the combustion. Compared to the baseline case at SOI=315^o CA *c.f.* Fig. 7 (b), NO_x emissions could be reduced by using a high included angle of the spray; however, the combustion efficiency at this SOI could be lowered as well. Therefore, the tradeoff was not improved under high included angle condition. In Fig. 9 (b), the low included angle showed local Φ_{max}=1.29 at SOI=315^o CA, leading to potentially much more NO_x emissions compared to the baseline case in Fig. 7 (b).

Conclusions

A multi-dimensional model was used to investigate the effects of late DI of iso-octane fuel with different injection timings on the fuel distribution in SCCI. It was found that the modelled fuel distributions showed a good agreement with the experiments. To the best of our knowledge, this is among very few detailed comparisons of model and experimental fuel distributions in this type of engine.

The fuel distributions were used to explain the observed experimental trends with injection timing obtained from firing tests in a nominally identical metal engine. With more retarded injection timing, the combustion efficiency and emissions of CO and uHC were improved by increasingly concentrated fuel distributions in the central regions and less fuel in the crevice volume, but NO_x emissions were increased due to the appearance of regions with excessively high equivalence ratios. The results emphasized the importance of the combustion efficiency versus NO_x tradeoff and suggested that it is likely to be highly dependent on the details of the geometry and flow conditions.

By examining the model results with different flow and injection parameters, such as swirl ratio, injection pressure and include angle of the spray, it was speculated that a high swirl ratio slowed the mixing, which could be detrimental to the combustion efficiency/NO_x tradeoff. Under a high injection pressure, the tradeoff could be potentially improved, while a low injection pressure showed a strongly adverse effect. A high included angle of the spray counteracted the effects of DI on the improvement of combustion efficiency. With a low included angle, the mixing was considerably slowed and the combustion efficiency/NO_x tradeoff was consequently deteriorated.

It should be noted that there was no combustion modelled in this study. In the reacting case, the flame may have strong effects on the spray structure and mixing, such as occurs in diesel engines. In HCCI engines, since the mixture is rather lean and injection timings considered in this study are relatively earlier than that in conventional diesel engines, it would be expected that injected liquid fuel is evaporated completely prior to the combustion event. There might be certain effects of low-temperature chemistry on the mixture distribution under late injection. The overall effects of flames on spray and mixture formation, however, are less significant in HCCI engines compared to diesel engines. Hence, this non-reacting study still can provide useful information for investigating HCCI engines.

Acknowledgements

This work was supported by the Australian Research Council under grant numbers DP110104763 and FT100100536. This research was undertaken on the NCI National Facility in Canberra, Australia, which is supported by the Australian Commonwealth Government. Drs John Dec and Magnus Sjöberg are thanked for their assistance with providing the experimental data and details.

References

[1] Thring, R. H., *SAE Technical Paper*, 892068, (1989).
[2] Dec, J. E., *Proceedings of the Combustion Institute* 32 (2):2727-2742, (2009).
[3] Dec, J. E., Sjöberg, M., *SAE Technical Paper*, 2003-01-0752, (2003).
[4] Dec, J. E., Sjöberg, M., *SAE Technical Paper*, 2004-01-0557, (2004).
[5] Sjöberg, M., Dec, J. E., *SAE Technical Paper*, 2006-01-0629, (2006).
[6] Hwang, W., Dec, J. E., Sjöberg, M., *SAE Technical Paper*, 2007-01-4130, (2007).
[7] Abraham, J., *International Journal of Automotive Technology*, 12 (5): 721-732, (2011).
[8] Heywood, J. B., "Internal Combustion Engine Fundamentals", McGraw-Hill, U.S., pp. 345, (1998).
[9] ANSYS CFX-Solver Release 13.0, *ANSYS CFX-Solver Theory Guide*, ANSYS Inc., (2010).
[10] ANSYS CFX-Solver Release 13.0, *ANSYS CFX-Solver Modelling Guide*, ANSYS Inc., (2010).
[11] Reitz, R. D., Diwakar, R., *SAE Technical Paper*, 870598, (1987).
[12] Naber J. D., Siebers D. L., *SAE Technical Paper*, 960034, (1996).
[13] Siebers D. L., *SAE Technical Paper*, 1999-01-0528, (1999).
[14] O'Rourke, P. J., "Collective drop effects on vaporizing liquid sprays", PhD Thesis, Princeton University, (1981).
[15] Som, S., Aggarwal, S. K., *Atomization and Sprays*, 19(9):885-903, (2009).
[16] Sjöberg, M., Dec, J. E., *SAE Technical Paper*, 2004-01-1900, (2004).